Experimental and theoretical *K* x-ray spectra of manganese

P. Jonnard, G. Giorgi, and C. Bonnelle
Laboratoire de Chimie Physique—Matière et Rayonnement, UMR CNRS 7614, Université Pierre et Marie Curie, 11 Rue Pierre et Marie Curie, 75231 Paris Cedex 05, France
(Received 4 June 2001; published 14 February 2002)

A high-resolution study of the *K* x-ray emission spectrum of the metal manganese is presented. The spectrum of the $3d^6 4s^1$ configuration is simulated with the help of a multiconfiguration Dirac-Fock program. Good agreement is obtained between the experimental and simulated shapes of the well resolved $K\alpha_{1,2}$ doublet as well as of the strongly asymmetrical $K\beta$ emission. The experimental intensity of $K\beta_5$ is larger than the predicted value because a mixing of the *s*, *p*, and *d* valence states exists in the solid. Satellite emissions, due to the transitions in doubly ionized atoms created by shake-off processes, are observed toward the higher energies of the normal emissions, at the predicted energies. In contrast, no radiative Auger satellite is observed toward the lower energies. We conclude that this process cannot be described in the shake approximation as previously assumed. The measured and theoretical $I(K\beta)/I(K\alpha)$ intensity ratios agree within 3%. Both are almost independent of the satellite emissions, while they vary appreciably with the external Mn configuration.

DOI: 10.1103/PhysRevA.65.032507 PACS number(s): 32.30.Rj, 32.70.−n

I. INTRODUCTION

Knowledge of atomic parameters is necessary to determine the strengths of excitation and ionization processes and of radioactive processes, electron capture, and internal conversion. Among these parameters, the fluorescence yields of the various shells *K*, *L*, *M*, . . . , the intensity ratios of the emissions $I(L)/I(K)$, $I(M)/I(L)$, . . . , and the intensity ratio of the $K\alpha$ and $K\beta$ emissions are the most important.

A large amount of work has been done for elements of atomic number $Z \leqslant 30$ on the theoretical and experimental determination of the intensity ratio $I(K\beta)/I(K\alpha)$ [1–7] and on its dependence upon chemical environment [8–12]. It has been suggested for $3d$ transition elements [13] that the $I(K\beta)/I(K\alpha)$ ratio is a linear function of the number of $3d$ electrons.

Most of the experimental data have been obtained by energy-dispersive x-ray spectrometry. Generally, they have been analyzed under the assumption that each of the $K\alpha$ and $K\beta$ emissions is expressed as a single Gaussian function. In some cases, an additional peak located toward the low energy of the $K\beta$ emission has been added [14]. The $I(K\beta)/I(K\alpha)$ intensity ratio has been deduced and an absolute accuracy of 1% or less is claimed for its determination. However, experimental values reported show important scatter. On the other hand, the fine structures in the $K\alpha$ and $K\beta$ emissions have been resolved by high-resolution x-ray spectroscopy and their dependence on the chemical environment has been investigated.

We have studied the Mn *K* spectrumn in order to analyze the characteristics of the Mn *K* x-ray normal (in the monoionized atom) and satellite emissions and to investigate the parameters that govern the precision of the determination of the $I(K\beta)/I(K\alpha)$ intensity ratio. By using a multiconfiguration Dirac-Fock (MCDF) code calculation, the normal and satellite emissions have been simulated for the Mn $(Ar)3d^n$ and $3d^n 4s^1$ or $3d^n 4s^2$ configurations with *n* varying between 6 and 4. The $I(K\beta)/I(K\alpha)$ ratio has been deduced. The simulation method and the computations are presented in Sec. II in comparison with the previous theoretical data. High-resolution spectral analysis of the Mn *K* x-ray emissions in the metal has been performed and $I(K\beta)/I(K\alpha)$ has been determined. The results are described in Sec. III. In Sec. IV, the experimental and theoretical data are compared and the shape and the intensity of the various emissions, in particular the relative intensity of the high- and low-energy satellites, are discussed.

II. CALCULATED X-RAY EMISSIONS

A. Methodology

The electric dipolar emissions that take place between the $1s$ and np inner subshells are calculated for manganese in the free atom and in various electronic configurations. A MCDF program is used to compute wave functions, energies, and transition probabilities [15]. The initial and final configurations of the emissions are obtained from the extended average level extension of the MCDF method coupled with the Slater transition state (method I). In this model, the vacancy is shared between both subshells and the correlation effects are minimized. Another weighting model is also used, in which to each initial or final configuration is assigned a weight equal to the statistical weight of the considered subshell (method II). The length and velocity forms of the transition matrix elements are used.

Because the interactions between the various *J* levels of the excited and ionized configurations are very fast, all the *J* levels of the initial configuration are populated statistically. Radiative emission is then the sum of all the lines that can occur between the various *J* levels of the initial and final configurations, each line being weighted by the statistical weight of the initial *J* level. This method was already used with success to interpret the shape of uranium x-ray emissions [16]. Each emission is characterized by its energy and its probability: the energy is either the energy of the most intense line or the *average* energy which is the barycenter of all the lines; the probability is either the maximum transition

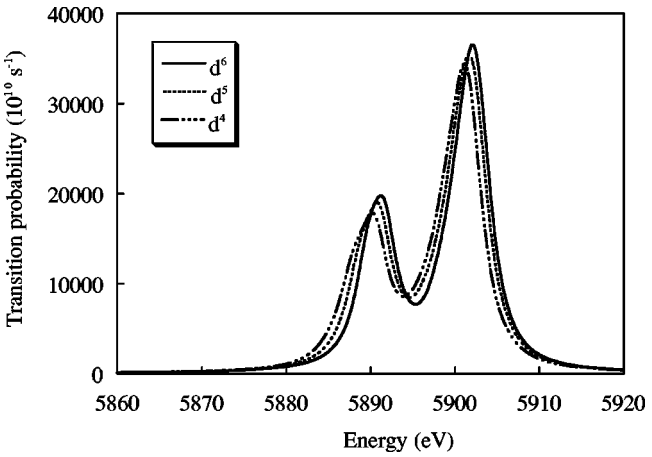

FIG. 1. $K\alpha_{1,2}$ simulated emission of Mn d^6, d^5, and d^4.

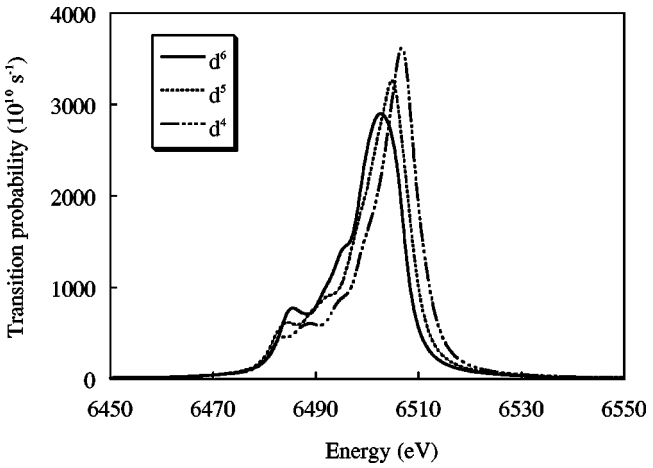

FIG. 2. $K\beta_{1,3}$ simulated emission of Mn d^6, d^5, and d^4.

rate or the *average* probability, which is the weighted sum of probabilities of all the lines.

Simulated emission is obtained by folding the theoretical probability of each line with a Lorentzian broadening function whose width results from the intrinsic lifetime and by calculating the weighted sum of all the lines. Finite experimental resolution is taken into account with a Lorentzian or Gaussian broadening function.

B. Simulation of Mn $K\alpha$ and $K\beta$ emissions

$K\alpha_{1,2}$ $(2p\rightarrow 1s)$ and $K\beta_{1,3}$ $(3p\rightarrow 1s)$ emissions are calculated from separate runs. Simulated spectra obtained for Mn (Ar)$3d^n$ with n varying from 6 to 4 are plotted in Figs. 1 and 2. Each emission results from several thousands of closely bunched lines. However, because the $2p$ spin-orbit coupling (11.1 eV) is large with respect to the $2p$-$3d$ interaction, the $K\alpha_1$ and $K\alpha_2$ peaks are well separated; their width is only 4 eV and their shape is almost symmetrical. In contrast, the $3p$-$3d$ interaction is greatly predominating; it creates a large multiplet splitting of the nonresolved $K\beta_{1,3}$ emission which spreads over about 20 eV. Due to the strong $3p$-$3d$ interaction, the energy broadening of $K\beta_{1,3}$ is governed by the energy distribution of the final state and not by the lifetime of states. The $K\beta_{1,3}$ emission is strongly asymmetrical toward the lower energies and the structures expected in this range vary with n.

We have listed in Table I for $K\alpha_1$, $K\alpha_2$ and $K\beta_{1,3}$ ($n=6$) the energies of the most intense line. They are compared to the differences of the inner subshell binding energies, calculated separately for each subshell. For $K\alpha_1$ and $K\alpha_2$, the energies of the maxima are near the experimental values [17]. For $K\beta_{1,3}$, the energy of the most intense line is located toward the higher energies and corresponds neither to the centroid of the emission nor to the experimental value. This is due to the large asymmetry of this emission.

TABLE I. Energies (eV) of normal and satellite emissions: (1) energy of the simulated spectrum maximum; (2) difference between the energies of the initial and final states; (3) experimental values from Ref. [17].

Normal	(1)	(2)	(3)
K-L_{II} (α_2)	5891.2	5897.0	5887.6
K-L_{III} (α_1)	5902.1	5908.2	5898.7
K-$M_{\mathrm{II,III}}$ $(\beta_{1,3})$	6502.4	6485.2	6490.4
K-$M_{\mathrm{IV,V}}$ (β_5)	6530.5		6535.4
Double ionization	(1)		(1)
KL_{I}-$L_{\mathrm{I}}L_{\mathrm{II,III}}$	5932	KL_{I}-$L_{\mathrm{I}}M_{\mathrm{II,III}}$	6549
$KL_{\mathrm{II,III}}$-$L_{\mathrm{II,III}}L_{\mathrm{II,III}}$	5931	$KL_{\mathrm{II,III}}$- $L_{\mathrm{II,III}}M_{\mathrm{II,III}}$	6564
KM_{I}-$M_{\mathrm{I}}L_{\mathrm{II,III}}$	5910	KM_{I}- $M_{\mathrm{I}}M_{\mathrm{II,III}}$	6511
$KM_{\mathrm{II,III}}$-$M_{\mathrm{II,III}}L_{\mathrm{II,III}}$	5912	$KM_{\mathrm{II,III}}$-$M_{\mathrm{II,III}}M_{\mathrm{II,III}}$	6498
Radiative Auger	(2)		(2)
K-$L_{\mathrm{II,III}}M_{\mathrm{I}}$	5745–5785	K-$M_{\mathrm{I}}M_{\mathrm{II,III}}$	6360–6395
K-$L_{\mathrm{II,III}}M_{\mathrm{II,III}}$	5770–5820	K-$M_{\mathrm{II,III}}M_{\mathrm{II,III}}$	6390–6430
K-$L_{\mathrm{II,III}}M_{\mathrm{IV,V}}$	5845–5870	K-$M_{\mathrm{IV,V}}M_{\mathrm{II,III}}$	6455–6480

TABLE II. Transition probabilities (10^{10} s^{-1}) of normal and satellite $K\alpha$ and $K\beta$ emissions calculated for Mn d^6, d^5, and d^4.

	$K\alpha_{1,2}$	Satellites			
Initial state	$1s^1$	$1s^13p^5$	$1s^13s^1$	$1s^12p^5$	$1s^12s^1$
d^6	47213	49223	47380	41166	47568
d^5	47187	49260	47359	41149	47547
d^4	47164	49305	47348	41138	47538
	$K\beta_{1,3}$	Satellites			
Initial state	$1s^1$	$1s^13p^5$	$1s^13s^1$	$1s^12p^5$	$1s^12s^1$
d^6	5801	5024	5748	7504	6493
d^5	5972	5199	5956	7748	6727
d^4	6195	5408	6204	8032	7002

TABLE III. Relative intensities of normal, satellite, and total $K\alpha$ and $K\beta$ emissions calculated for Mn d^6, d^5, and d^4.

	$K\alpha_{1,2}$	Satellites				
Initial state	$1s^1$	$1s^13p^5$	$1s^13s^1$	$1s^12p^5$	$1s^12s^1$	Total
d^6	43946	2151	692	338	128	47255
d^5	43922	2153	691	337	128	47231
d^4	43900	2155	691	337	128	47211
	$K\beta_{1,3}$	Satellites				
Initial state	$1s^1$	$1s^13p^5$	$1s^13s^1$	$1s^12p^5$	$1s^12s^1$	Total
d^6	5400	219.5	83.9	61.5	17.5	5782
d^5	5559	227.2	87.0	63.5	18.2	5955
d^4	5766	236.3	90.6	65.9	18.9	6178

The $K\beta_5$ emission is expected at 6531 eV. From the theoretical calculation in the free ion, its relative intensity should be very weak, less than 0.1% of $K\beta_{1,3}$. However, because the $3d$ electrons are strongly mixed with the $4sp$ electrons in the solid, one expects that an emission from p character states, mixed with the $3d$ states, will be observed in the metal at the position of $K\beta_5$ with an intensity clearly higher than that calculated.

As seen from Figs. 1 and 2, the energies of the $K\alpha_{1,2}$ and $K\beta_{1,3}$ emissions vary with n in an opposite manner. When the oxidation degree of Mn increases, i.e., when n decreases, $K\alpha_{1,2}$ shifts toward lower energies while $K\beta_{1,3}$ shifts in the opposite direction. On the other hand, the average probability of the $K\alpha_{1,2}$ emission decreases by less than 0.1% with decreasing n while the probability of the $K\beta_{1,3}$ emission increases by about 10% with decreasing n (cf. Table II).

C. Simulation of satellites

High-energy satellites are due to transitions in doubly ionized atoms. Indeed, an additional inner hole generally shifts the transition toward the higher energies and the shift is greater as the additional hole is present in a deeper shell. *Ab initio* computations of the energies of the maximum transition rate (cf. Table I) as well as the energy distributions have been performed for the *K* satellites. The satellites arising from the *KM* double initial ionization are difficult to resolve from diagram lines because of the high multiplicity of the configurations with a supplementary hole. Thus one expects that these satellites might be only a bump on the high-energy side of the emission lines. In contrast, the satellites due to *KL* doubly ionized atoms are clearly separated from the normal emission.

The calculated average transition probabilities of the $K\alpha$ and $K\beta$ satellites are indicated in Table II, compared to the probabilites of the $K\alpha_{1,2}$ and $K\beta_{1,3}$ emissions. The probabilities of the corresponding normal and satellite emissions are close. The intensity of an emission depends both on the transition probability and on the number of atoms in the initial state, i.e., on the number of atoms in a doubly ionized state in the case of the satellites. For *K* emissions, only double ionization by shake-off processes is to be taken into account. For the Mn atom, the production percentage of multivacancy states by the shake-off effect relative to single vacancy production, P_{KX}, is 0.82% for the $2p$ subshell and 4.37% for the $3p$ subshell [18]. It is at least three times weaker for the $2s$ and $3s$ subshells, respectively.

By multiplying the transition probability of each normal emission by $(1-\Sigma P_{KX})$ and that of each double-ionization satellite by its P_{KX} factor, we have determined the relative intensities of the normal and satellite emissions. They are reported in Table III. We also give in Table III the sums of the relative intensities of the normal and satellite $K\alpha$ and $K\beta$ emissions. It is remarkable that these sums differ very little from the transition probabilities of the $K\alpha_{1,2}$ and $K\beta_{1,3}$ emissions, reported in Table II. This is because the transition probabilities of all the $K\alpha$ or $K\beta$ emissions are close together and the relative intensities of the satellites are weak.

In the $3d$ transition element range, satellites due to radiative Auger effects (RAE's) have been studied extensively. According to theoretical predictions based on the shake model [18], the *K-MM* RAE components should be the most probable and their relative probabilities with respect to the $K\beta_{1,3}$ probability should be about 4%. Experimentally, for transition metals, the intensity of *K-MM* satellites is two orders of magnitude less than the intensity of the $K\beta_{1,3}$ peak [19], that is to say, clearly weaker than the predicted value. We have calculated the energies of the *K-LM* and *K-MM* components (cf. Table I). They each extend over about 25–40 eV. As a consequence of their spread and their weak intensity these transitions are difficult to observe.

D. $I(K\beta)/I(K\alpha)$ intensity ratio

First, we have calculated the $I(K\beta_{1,3})/I(K\alpha_{1,2})$ ratio for different configurations from the average probabilities calculated for each emission as indicated above. We have used the two methods of weighting and the length and velocity forms of the matrix elements. Results are presented in Table IV and compared to recent published values [7] and to the values proposed by Scofield [18]. The agreement is good between these values and the results we obtained by the weighting method based on the Slater transition states (method I). Differences of 0.0038, i.e., about 3%, exist between the $I(K\beta_{1,2})/I(K\alpha_{1,2})$ ratios calculated with the length and ve-

TABLE IV. $I(K\beta_{1,3})/I(K\alpha_{1,2})$ intensity ratio. Method I: by building the Slater transition state; method II: by weighting each state by its statistical weight. *l* denotes the length form of the transition matrix element, *v* denotes the velocity form.

	Other work		Method I		Method II	
	l	*v*	*l*	*v*	*l*	*v*
$3d^6 4s^1$	0.1326 [a]	0.1307 [a]	0.1328	0.1289	0.1228	0.1207
$3d^6$			0.1328	0.1290	0.1229	0.1208
$3d^5 4s^2$	0.1361 [a]	0.1342 [a]	0.1361	0.1323	0.1260	0.1239
		0.1339 [b]				
$3d^5$			0.1367	0.1328	0.1266	0.1244

[a]Reference [7].
[b]Reference [18].

locity forms. Concerning the electronic configurations, a variation of 3% exists between d^6 and d^5. In contrast, between $3d^6$ and $3d^6 4s^1$ the change is negligible and it is 0.4% between $3d^5$ and $3d^5 4s^2$. Thus the electronic configuration intervenes essentially depending on the number of *d* electrons. This is because the $3d$ electrons play an important role in the intensity of the $K\beta$ emission as already mentioned in the previous section.

The $I(K\beta_{1,3})/I(K\alpha_{1,2})$ ratio increases with decreasing *n*. The variation of the ratio between two electronic configurations is a relative datum known with an uncertainty in the fourth digit. This variation can be used to obtain the value of the ratio for a compound if the Mn oxidation degree in this compound is known.

To determine the $I(K\beta)/I(K\alpha)$ ratio, all the *K* normal and satellite emissions must be taken into account. From experimental results described below, only the double-ionization satellites have sufficient intensity to affect the ratio notably. When the sums of the $K\alpha$ and $K\beta$ emissions are taken into account (cf. Table IV), $I(K\beta)/I(K\alpha)$ differs from $I(K\beta_{1,3})/I(K\alpha_{1,2})$ by -0.0005. This difference is clearly smaller than the difference due to the form of the matrix element.

III. EXPERIMENT

A. Experimental details

Manganese metal plates of 99.9% purity (Alfa Aesar) were used. The samples were fixed on a water-cooled sample holder. This sample holder is the anode of an ultrahigh-vacuum x-ray tube. The current density was less than 1 mA/cm^2. Special care was taken to consider only the data not showing an evolution in time.

The spectra were recorded by using a 50 cm radius bent crystal vacuum spectrometer [20] equipped with various crystalline slabs: LiF 200 used at the first reflection order and quartz $11\bar{2}0$ used at the second reflection order. Because of its high luminosity, LiF is used for the analysis of weak intensity emissions. The quartz $11\bar{2}0$ crystal is less luminous but its resolution is better, making the $K\alpha_{1,2}$ doublet well resolved. A polyethylene-windowed Ar-CH_4 gas-flow proportional counter was placed behind an adjustable slit situated on the Rowland circle. The spectra were recorded over a wide enough region to precisely take into account the background. The spectral distribution of the continuum background is obtained from analysis of the spectrum emitted by an element of adjacent atomic number having no discrete emission in the spectral range considered.

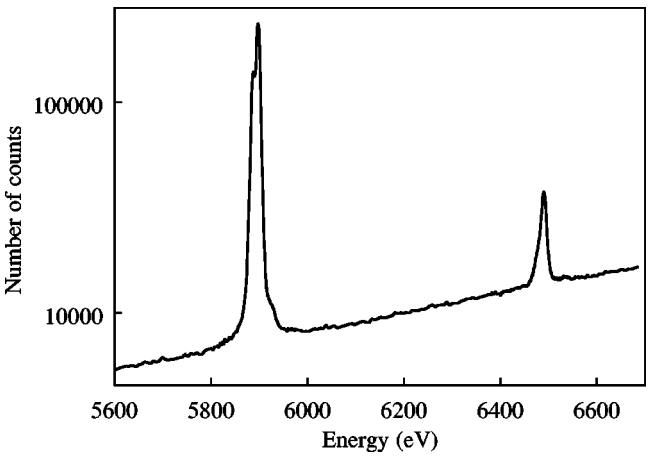

FIG. 3. Experimental *K* emission spectrum of metal Mn obtained with a LiF (200) crystal at the first reflection order. The intensities are plotted on a logarithmic scale.

The Mn *K* spectrum is excited with electrons whose energy is about 1.5 times the *K* ionization threshold, i.e., 9.5 keV. In these conditions, the ionization process is favored with respect to the bremsstrahlung emission process. On the other hand, the energy of the ionizing electrons is sufficient for the sudden approximation to be valuable and the probability of double ionization by the shake-off effect fits the predicted value.

B. Mn *K* emission spectrum

The Mn *K* spectrum analyzed with the LiF crystal is plotted in Fig. 3 on a logarithmic scale to enhance the weak intensity emissions. No structure is seen toward the lower energies of the $K\alpha_{1,2}$ doublet and the shape of the spectrum is characteristic of pure x-ray emission in this energy range. In contrast, a structure is observed towards the higher energies of $K\alpha_{1,2}$ at the position calculated for the *KL-LL* double-ionization satellites. The $K\beta_{1,3}$ emission is asymmetrical toward the lower energies and no satellite is seen in this range. Weak intensity $K\beta_5$ emission is observed at the energy expected from the previous experimental data [8].

In Fig. 4, the well resolved $K\alpha_{1,2}$ doublet, analyzed with a quartz $11\bar{2}0$ crystal, is plotted compared to the simulated spectrum. The continuous emission due to bremsstrahlung has been removed from the experimental curve, which agrees perfectly with the previous high-resolution spectrum of metal Mn [21]. Both curves of Fig. 4 have been adjusted to the maximum of the $K\alpha_1$ emission by shifting the simulated curve toward the lower energies (cf. Table I). Good agreement exists between the two curves. Indeed, the $K\alpha_1$-$K\alpha_2$ splitting, the relative intensities, and the shapes of $K\alpha_1$ and $K\alpha_2$ emissions are similar.

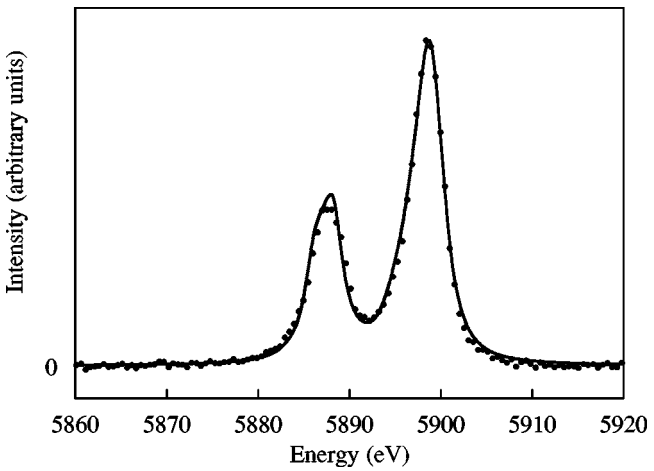

FIG. 4. Experimental (dots) and simulated (continuous line) $K\alpha_{1,2}$ emission of metal Mn.

Experimental and simulated $K\beta_{1,3}$ emissions are plotted in Fig. 5. They are adjusted at the top of the emission. The simulated curve reproduces well the low-energy tail of the experimental curve, which spreads over about 20 eV. Toward the higher energies, the experimental spectrum is above the simulated one. The difference can be explained by the presence of double-ionization *KM-MM* satellites. They have been simulated and are plotted in Fig. 5. The energy shift between the experimental and simulated satellites is different from that between the normal emissions. This difference has been taken into account in the figure. Because of the high multiplicity of the configurations with a supplementary hole, the doubly ionized *KM* satellites are not resolved and appear only as a tail on the high-energy side of the $K\beta_{1,3}$ emission.

C. $I(K\beta)/I(K\alpha)$ intensity ratio

Intensity ratios of different energy emissions must be determined with the geometrical conditions of the spectrometer making the lighting of the detector the same in both energy ranges. This condition is strictly satisfied in the focal plane, i.e., in the plane perpendicular to the crystal surface at its center. Consequently, the height of the x-ray beam was greatly reduced by positioning a diaphragm just ahead of the crystal and only its central part was used. That reduces the luminosity and the measurements were made with the LiF crystal.

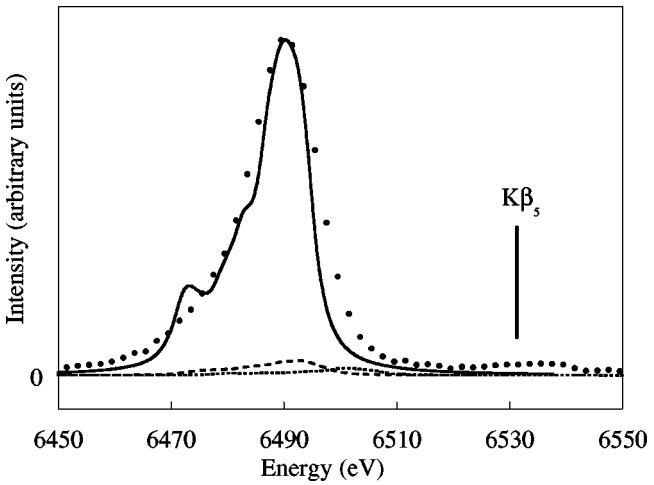

FIG. 5. Experimental (dots) and simulated (continuous line) $K\beta_{1,3}$ emission of metal Mn; *KM-MM* satellites (broken lines). The position of $K\beta_5$ is indicated.

The spectral range spreads over about 1000 eV. A corrected spectrum is obtained by taking into account the continuous variation with energy of the following parameters: the reflectivity of the crystal, the self-absorption of the radiation in the sample, and the response of the detector. For each emission, the intensity is determined by integrating the region including the normal emission and the low- and high-energy satellites. Numerous determinations were made, by varying the extension of the energy range and the method of background subtraction. Finally, the value obtained is

$$I(K\beta)/I(K\alpha) = 0.134 \pm 0.004.$$

As is well known, the $3d$ electron number is close to 6 in metallic Mn [22]. The experimental value has to be compared to the ratio calculated for the $3d^6 4s^1$ configuration, including the $K\beta_5$ emission contribution determined for the solid.

IV. DISCUSSION

Comparison between the simulated and experimental spectra has shown that the normal lines can be reasonably reproduced. In particular, the low-energy tail of the observed $K\beta_{1,3}$ peak agrees well with the calculation. Previously, the asymmetry of the $K\beta_{1,3}$ emission had been described by the presence of a structure, denoted $K\beta'$, interpreted as due to the interaction between the electrons in the incomplete $3d$ subshell and the $3p$ hole [8,23]. Our calculations, carried out for free atoms, support this interpretation. Indeed, the $3p$-$3d$ exchange energy, about 10 eV, is the dominant interaction. It is much larger than the $3p$ spin-orbit splitting and the energy splitting due to the ligand field (≈ 1 eV for the Mn d orbitals in a cubic field). This explains why the simulation from atomic calculations fits well the experimental data for the solid.

The shape of the $K\beta_{1,3}$ emission is governed by the large multiplet splitting of the $3p$-$3d$ configuration, i.e., by the energy distribution of the final state. Thus, it depends on the number of unpaired $3d$ electrons. Indeed, the energy separation between the $K\beta'$ structure and $K\beta_{1,3}$ and the intensity ratio of $K\beta'$ and $K\beta_{1,3}$ are very sensitive to the oxidation degree of Mn, i.e., to the chemical environment of the emitting atom.

It is well known that around $Z=24$ (Cr) there is an enhancement in the relative intensity of the $K\beta_5$ emission which is not predicted by the theoretical values obtained for free atoms. Experimentally, the $K\beta_5$ emission can contribute up to 4.5% of the intensity of the $K\beta$ emission and is very sensitive to environmental effects. For solids with $Z \leqslant 29$, the $3d$ wave function is not fully localized on the atom and the $3d$ orbital overlaps with the valence band. This is composed of $4sp$ character states and mixing exists between these

states and the $3d$ states. The probability ratio of the electric dipole transition $4p \rightarrow 1s$ to the electric quadrupole transition $3d \rightarrow 1s$ in transition elements is on the order of 100. Thus, the intense part of the $K\beta_5$ band is ascribed to $4p \rightarrow 1s$ transitions. This explains the enhancement of the $K\beta_5$ intensity with respect to the intensity expected for electric quadrupole transition and the strong dependence of the $K\beta_5$ relative intensity on the chemical environment.

In our experimental conditions, satellites due to doubly ionized states created by shake off are observed toward the higher energies of $K\alpha_{1,2}$ and $K\beta_{1,3}$. Only the *KL-LL* double-ionization satellites are partially resolved from the $K\alpha_{1,2}$ doublet in Fig. 3. For $K\beta_{1,3}$, *KM-MM* satellites appear only as a high-energy tail. In contrast, no radiative Auger satellite is seen in the pure metal Mn *K* spectrum. Consequently, double-ionization satellites are clearly more intense than the radiative Auger satellites. This result shows that the RAE probability is not well described in the shake approximation, in agreement with experiments in which the RAE intensity is much weaker than the predicted value. A different model is necessary to describe this process.

To conclude, from our analysis of the Mn *K* spectrum, it appears that the dependence of the $I(K\beta)/I(K\alpha)$ intensity ratio on the physicochemical characteristics is more significant than the changes brought about by the contribution of the satellite emissions.

ACKNOWLEDGMENTS

This work was supported by the Bureau National de Métrologie under Grant No. 99-258. The authors wish to thank Dr. Bé and Dr. Lépy for helpful discussions.

[1] V. W. Slivinsky and P. J. Ebert, Phys. Rev. A **5**, 1581 (1972).
[2] S. I. Salem, T. H. Falconer, and R. W. Winchell, Phys. Rev. A **6**, 2147 (1972).
[3] F. Bodart, G. Deconninck, and S. Wilk, X-Ray Spectrom. **4**, 161 (1975).
[4] K. F. Heinrich, C. E. Fiori, and R. L. Myklebust, J. Appl. Phys. **50**, 5589 (1979).
[5] A. Perujo, J. A. Maxwell, W. J. Teesdale, and J. L. Campbell, J. Phys. B **20**, 4973 (1987).
[6] L. Rebohle, U. Lehnert, and G. Zschornack, X-Ray Spectrom. **25**, 295 (1996).
[7] S. Raj, H. C. Padhi, and M. Polasik, Nucl. Instrum. Methods Phys. Res. B **160**, 443 (2000).
[8] K. Tsutsumi, H. Najamori, and K. Ichikawa, Phys. Rev. B **13**, 929 (1976).
[9] G. Brunner, M. Nagel, E. Hartmann, and E. Arndt, J. Phys. B **15**, 1517 (1982).
[10] G. Peng, F. M. F. de Groot, K. Hmlinen, J. A. Moore, X. Wang, M. M. Grush, J. B. Hasting, D. P. Siddons, W. H. Armstrong, O. C. Mullins, and S. P. Cramer, J. Am. Chem. Soc. **116**, 2914 (1994).
[11] Q. Qian, T. A. Tyson, C.-C. Kao, J.-P. Rueff, F. M. F. de Groot, M. Croft, S.-W. Cheong, M. Greenblatt, and M. A. Subramanian, J. Phys. Chem. Solids **61**, 457 (2000).
[12] S. D. Gamblin and D. S. Urch, J. Electron Spectrosc. Relat. Phenom. **113**, 179 (2001).
[13] T. Mukoyama, K. Taniguchi, and H. Adachi, X-Ray Spectrom. **29**, 426 (2000).
[14] M.-C. Lépy, J. Plagnard, and J. Morel, Nucl. Instrum. Methods Phys. Res. A **339**, 241 (1994).
[15] J. Bruneau, J. Phys. B **16**, 4135 (1983).
[16] C. Bonnelle, P. Jonnard, C. Barré, G. Giorgi, and J. Bruneau, Phys. Rev. A **55**, 3422 (1997).
[17] Y. Cauchois and C. Sénémaud, *International Tables of Selected Constants: Wavelengths of X-ray Emission Lines and Absorption Edges* (Pergamon Press, Oxford, 1978).
[18] J. H. Scofield, Phys. Rev. A **9**, 1041 (1974).
[19] O. Keski-Rakhonen and J. Ahopelto, J. Phys. C **13**, 471 (1980).
[20] C. Bonnelle, F. Vergand, P. Jonnard, J.-M. André, P.-F. Staub, P. Avila, P. Chargelègue, M.-F. Fontaine, D. Laporte, P. Paquier, A. Ringuenet, and B. Rodriguez, Rev. Sci. Instrum. **65**, 3466 (1994).
[21] H. W. Schnopper, Phys. Rev. **154**, 118 (1967).
[22] D. A. Papaconstantopoulos, *Handbook of the Band Structure of Elemental Solids* (Plenum, New York, 1986).
[23] K. Tsutsumi and H. Nakamori, J. Phys. Soc. Jpn. **25**, 1418 (1968).